Applied Catalysis B: Environmental 259 (2019) 118048

Contents lists available at ScienceDirect

Applied Catalysis B: Environmental

journal homepage: www.elsevier.com/locate/apcatb

Electrochemical reduction of NO_x species at the interface of nanostructured Pd and PdCu catalysts in alkaline conditions

J. Soto-Hernández[a], C.R. Santiago-Ramirez[a], E. Ramirez-Meneses[b], M. Luna-Trujillo[a], Jin-An Wang[c], L. Lartundo-Rojas[d], A. Manzo-Robledo[a,*]

[a] Instituto Politécnico Nacional, Laboratorio de Electroquímica y Corrosión, AIP-ESIQIE-IPN, UPALM, Zacatenco, C.P. 07738, Ciudad de Mexico, Mexico
[b] Departamento de Ingeniería Química, Industrial y de Alimentos, Universidad Iberoamericana, Prolongación Paseo de la Reforma 880, Lomas de Santa Fe, Ciudad de México, C.P. 01219, Mexico
[c] Laboratorio de Catálisis y Materiales, Instituto Politécnico Nacional, UPALM, Zacatenco, CP. 07738, Ciudad de Mexico, Mexico
[d] Centro de Nanociencias y Micro y Nanotecnologías, Instituto Politécnico Nacional, UPALM, Zacatenco, CP. 07738, Ciudad de Mexico, Mexico

ARTICLE INFO

Keywords:
NO_x reduction-interfacial-process
Electro-catalysis
Pollution control
Nanoparticles
DEMS

ABSTRACT

Electrochemical reduction of NO_x species such as nitrates (NO_3^-), nitrites (NO_{2-}), nitric oxide (NO), nitrogen dioxide (NO_2) and their mixtures, was studied at the interface of palladium (Pd) and palladium-copper (PdCu) nanoparticles supported on carbon Vulcan (C). The electro-catalysts were synthesized by impregnation route with a low noble metal content of 5% wt. Pd and 2.5% wt. Pd for the mono and bi-metallic electrocatalyst, respectively. It was found by XRD analysis the formation of a solid solution in the bi-metallic catalyst and the TEM analysis suggest that the incorporation of copper decreases the particle size from 12 to 3 nm in comparison with its counterpart free of copper. Also, XPS technique verify the presence of Pd and Cu species in their metallic-oxidation states. Linear sweep and cyclic voltammetry techniques were used for the evaluation of the electrochemical NO_x reduction, using alkaline solutions of NO_2^- or NO_3^- saturated with NO_2 (synthesized in-situ) and NO (from commercial source). The results showed that the catalytic-activity at the current versus potential (i-E) characteristics improves significantly due to the presence of copper (as also demonstrated by CO-stripping-electrochemical active surface area calculations), inhibiting the process associated with the hydrogen evolution reaction. It is also noted in this work that the reduction faradic-current is c.a. 6 times higher at saturated solutions with NO and NO_2. The NO_x species were reduced mainly to nitrogen, ammonia and hydrazine as confirmed using on-line differential electrochemical mass spectrometry (DEMS) during steady-state experiments.

1. Introduction

Nowadays pollution control and pollutants elimination from efficient and low-cost processes is a topic of great impact. The main pollutants emitted from power plants, car engines and chemical industry are nitrogen oxides NO_x (x = 1, 2, 3). In the atmosphere, NO reacts with oxygen to form $NO_{2(g)}$ that is an irritating acid gas. Also, it can further react with OH^- radicals to give nitric acid producing the so-called acid rain and contributing to the greenhouse effect [1]. Whereas, nitrate pollution in ground waters is derived from anthropogenic activities, stormwater and discharge wastewater. Nitrate in drinking water can generate methemoglobinemia ("blue baby syndrome") which is caused by nitrite in the human gastrointestinal tract [2] and is also been implicated in harmful impacts to humans [3,4]. In order to safeguard human health, the World Health Organization (WHO) suggested a maximum contaminant level (MCL) of 50 mg/l NO_3^- in drinking water. However, it is not enough, and many severe regulations must be introduced in the future. For this reason, treatments for their elimination (or control) must be considered. In this context, several approaches for NO_x mitigation have been proposed: lean NO_x trap (LNT) [5]; hydrocarbon selective-catalytic reduction (HC-SCR) [6,7]; selective-non-catalytic reduction (SNCR) [8,9]; NH_3-SCR; and SCR [10]. These methodologies have advantages and disadvantages; for example, the catalysts are active (only) at high temperatures (above 250 °C). In this context, electrochemical processes offer advantages such as eliminating the requirement for chemicals before and after the treatment, removing a small area occupied by the plant, disposing of sludge generation and low investment costs [11,12]. On the other hand, the mechanisms for electrochemical conversion of nitrate to nitrogen gas are highly complex, due to the numerous reactions involved in the process. Besides,

* Corresponding author.
E-mail address: amanzor@ipn.mx (A. Manzo-Robledo).

https://doi.org/10.1016/j.apcatb.2019.118048
Received 18 March 2019; Received in revised form 28 July 2019; Accepted 1 August 2019
Available online 08 August 2019
0926-3373/

products and stable intermediates are affected by electrode composition, crystal structure, pH and supporting electrolyte [13,14]. Therefore, the development of an active, selective and stable catalyst is necessary to maximize the NO_x electro-catalytic reduction. In this respect, several studies have been carried out using different systems composed of mono-metallic (Ir, Pt, Rh, Ru, Pd, Cu, Ni, Ag, Au) and bi-metallic catalysts (CuSn [15], PtCu [16] PdCu [17,18], CuNi [19], PdSn [20]). Among these materials, palladium and platinum have been mainly used for nitrate reduction due to their interfacial hydrogen evolution slow-kinetic. Likewise, copper electrodes exhibit a good selectivity to nitrogen [21,22].

In this work, an electrochemical approach for the NO_x reduction (NO_3^-, NO_{2-}, NO and NO_2) was carried out using synthesized carbon supported palladium and palladium–copper nanoparticles from impregnation route. It was found that the interfacial interaction under alkaline condition involved two sequences or scenarios: i) the reduction of nitrate to nitrite and ii) the interaction of the gas in turn at the bulk solution, producing other species that react at the electrode interface. Interestingly, the coupling with on-line DEMS (differential electrochemical mass spectroscopy) demonstrated that the generated species during the reduction reaction were N_2, N^+, $NH_3^-$and N_2H_4 with hydrogen at more negative potentials.

2. Experimental section

2.1. Synthesis of palladium and copper nanoparticles

Palladium (Pd) and palladium-copper (PdCu) nanoparticles were synthesized by impregnation method, using Copper (II) acetylacetonate ($Cu(C_5H_7O_2)_2$, Sigma Aldrich 99%)) and palladium (II) acetylacetonate ($Pd(C_5H_7O_2)_2$, Sigma Aldrich 99%) as precursors and polyvinylpyrrolidone (PVP, average mol wt 40,000, Sigma Aldrich) as stabilizer. All reagents were used without further purification. To prepare the catalysts, 52 mg of $Pd(C_5H_7O_2)_2$ or 26 mg of $Pd(C_5H_7O_2)_2$ and 35 mg of $(Cu(C_5H_7O_2)_2$ (for mono-metallic or bi-metallic catalyst, respectively) were dissolved in 30 mL of ethanol (Fermont, 99.9%) and mixed using PVP (5%wt respect to the palladium precursor) dissolved in 50 mL of ultrapure water (Millipore Milli-Q system, > 18 MΩ) in a 250 mL three-neck flask. The mixture was heated at 75 °C and kept under reflux with stirring in an argon atmosphere for 3 h. The color of the solution turned from orange to black-brown during the reaction. To prepare the carbon-supported catalyst, 30 mL of ethanol was added to carbon Vulcan (XC-72) and sonicated for 30 min. The mixture was added into the as-obtained Pd or PdCu colloidal solutions. Then, the solvent was evaporated under vacuum at 60 °C during 2 h using a rotatory evaporator (IKA RV10) at 150 rpm. The obtained black powder was filtered and rinsed with water and ethanol until neutral pH remained. At last, the powders were heat-treated at 300 °C under argon atmosphere for 3 h.

2.2. Synthesis of nitrogen dioxide (NO_2)

The nitrogen dioxide synthesis was carried out in-situ and then it was injected into the cell-reactor (in a similar way the $NO_{(g)}$ was injected into the reactor) Fig. 1. For this purpose, 0.75 g of metallic copper were mixed with 6 mL of concentrated nitric acid in a flask. A color change of the solution from green to red/brown was observed, indicating the presence of nitrogen dioxide (NO_2). The as-obtained gas was combined with argon in a 9:1 relation (90%vol. Ar-10%vol.NO_2). The initial green color is associated with the copper when ligated by nitrate ions in a high concentration in the acid [23], Eq. (1).

$$Cu_{(s)} + 4HNO_{3\,(aq)} \rightarrow Cu(NO_3)_{2\,(aq)} + 2NO_{2\,(g)} + 2H_2O_{(l)} \quad (1)$$

2.3. Morphological and structural characterization

Analysis of X-ray diffraction (XRD) for the samples in this study was collected from 15 to 90° (2θ) in a D2 Phaser Bruker diffractometer (Cu Kα radiation, λ_{Cu} = 1.5406 Å) in Bragg-Brentano theta-theta configuration. Rietveld refinements were carried out using TOPAS V5 software where a double-Voight approach model was selected to estimate crystallite size. The catalysts (Pd/C and PdCu/C) were also analyzed by transmission electron microscopy (TEM) using a JEOL microscope (JEM-2100). Samples were collected and sonicated in ethanol. A few droplets of ethanol suspension were placed onto a carbon-coated copper grid and dried in air at room temperature. Compositional and oxidation states of the catalysts were obtained by X-ray photoelectron spectroscopy (XPS) in a Thermo Scientific K-Alpha X-ray photoelectron spectrometer with a monochromatized AlKα X-ray source (1487 V). General and high-resolution spectra were collected using an X-ray spot size of 400 μm^2 at 160 and 40 eV pass energy, respectively. The samples remain in the pre-chamber for 10 h and subsequently transferred to the analytical chamber with a base pressure of 1×10^{-9} Torr. Core level spectra were deconvoluted with AVANTAGE v5.97 software from Thermo Fisher Scientific by means of Shirley-type background subtraction and a pseudo-Voigt function with Gaussian (70%)-Lorentzian (30%) for each component.

2.4. Electrochemical-DEMS characterization

The electrochemical measurements were performed using a potentiostat-galvanostat (VersaStat 3) in a three-standard electrochemical reactor with a carbon rod as a counter electrode (CE), a reversible hydrogen electrode (RHE) as a reference, and glassy carbon (GC) coated with the catalysts in turn as the working electrode. The GC electrode (geometric area of 0.196 cm^2) was polished with a 0.05 μm Al_2O_3 slurry to a mirror finish. A suspension (1 mL) was prepared by adding 5 mg of catalyst (PdCu/C or Pd/C) to a solution composed of 20% vol. isopropanol, 79. 8% vol. of ultrapure water (> 18 MΩ) and 0.2% vol. Nafion and sonicated for 60 min. Then 5 μL of the prepared suspension was deposited onto the surface of the polished GC and then dried under argon atmosphere. The electrochemical experiments were performed at room temperature and the solutions were purged with argon for 15 min prior to electrochemical analysis. Cyclic voltammetry was performed in 0.5 M NaOH solution as supporting electrolyte at different concentration of nitrates (NO_3^-) and nitrites (NO_{2-}) ions from 0.001 to 1.0 M at a scan rate of 20 mVs^{-1}. For the analysis of NO (INFRA 10% NO, 90% Ar) and NO_2 electrochemical reduction, the electro-catalysts were evaluated in a solution of 0.5 M NaOH at 25 °C saturated with the gas in turn.

A Differential electrochemical mass spectrometry (DEMS) cell-device with a three-electrode system was used for recording the ionic current-potential characteristics during the faradic process. The inlet system between the cell and the vacuum consisted of a porous membrane (thickness 60 μm, 0.1 μm pore size, 50% porosity). The reference electrode was a reversible hydrogen electrode (RHE), and the counter electrode a platinum wire. A glassy carbon disk (3 mm in diameter) was used as the working electrode. The ionic current (mass signal) for selected mass to charge ratios (*m/z*) were recorded simultaneously with the current versus potential characteristic at a scan rate of 2 mVs^{-1} in NO saturated electrolyte (15 min), from 0.7 to −0.9 V/RHE. For this purpose, the electrochemical cell was connected to the quadrupole mass spectrometer (Prisma Plus™ QMG220) for the isolation of the ion source from the reactor, forming a small pre-chamber (working pressure of ca. 4×10^{-5} mbar).

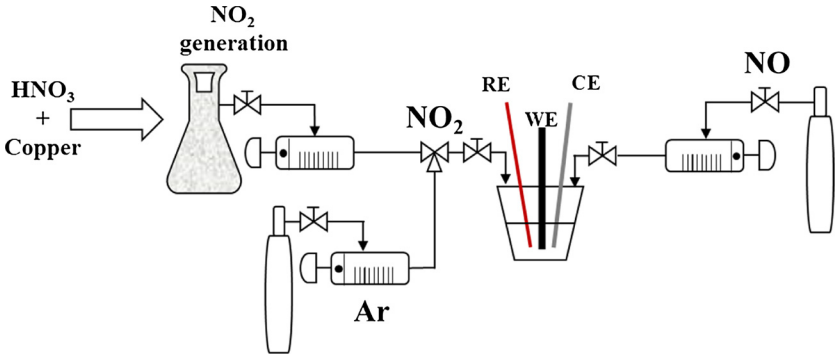

Fig. 1. Schematic representation of the experimental setup for NO and NO_2 (synthesized) coupling to the electrochemical cell.

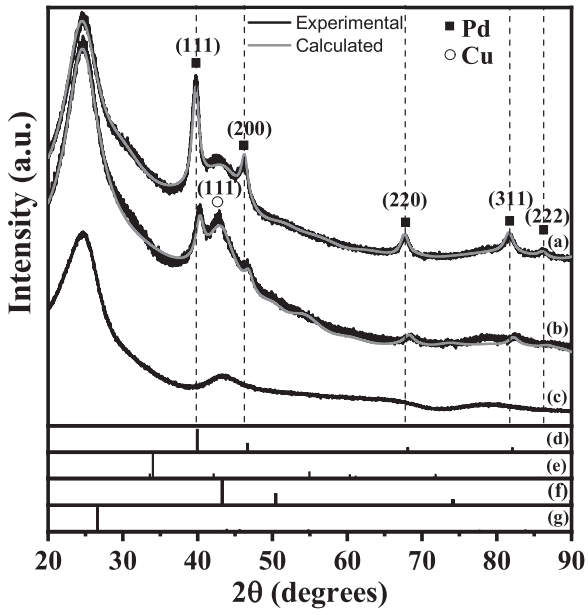

Fig. 2. X-ray diffraction pattern of (a) PdCu/C (b) Pd/C, (c) carbon vulcan XC-72R and powder diffraction patterns (ICDD) of (d) Pd, (e) PdO, (f) Cu and (g) carbon.

3. Results and discussions

3.1. Morphological and compositional analysis

X-ray diffraction (XRD) technique was used for the phase identification in the Pd/C and PdCu/C catalysts and carbon Vulcan (support), Fig. 2(a–c). Fig. 2a corresponds to the mono-metallic Pd/C pattern and exhibits five characteristic diffraction peaks at 40.1°, 46.6°, 68.09°, 82.1° and 86.5° (2θ) corresponding to (111), (200), (220), (311) and (222) planes of the face-centered cubic (FCC) structure of palladium. Two metallic phases, palladium and copper, were identified in PdCu/C catalyst (Fig. 2b). The comparison between the XRD patterns of Pd/C and PdCu/C catalysts is shown in Fig. 3, where a displacement in palladium reflections was found. In contrast, the position of Vulcan diffraction peak (24.7°) was the same in both samples; therefore, this phase can be considered as an internal standard to relate the palladium displacements in 2-theta with a structural change. The displacements observed in palladium reflections are a consequence of a change in lattice constant due to palladium substitution by copper atoms. This behavior was also reported by Xiong et al. with different molar ratios Pd:Cu, where the palladium diffraction peaks shift to higher angles when the copper concentration was increased [24–26]. In such a way, Rietveld refinements were done considering the palladium occupancy shared with copper atoms. The Rietveld refinement results (Table 1) confirm a smaller lattice constant for palladium in PdCu/C, in comparison with Pd/C. The average crystallite size of the mono-metallic Pd was 5.64 nm, whereas for bi-metallic sample, palladium crystallite size was 4.81 nm. These results are in agreement with the catalytic performance obtained in the electrochemical measurements (see Section 3).

In addition, Fig. 4(a–d) shows TEM micrographs and the corresponding particle size-distribution of Pd and Pd-Cu catalysts. From Fig. 4a, it can be seen nanoparticles with spherical morphology dispersed on Vulcan carbon surface with a particle size distribution of 12 ± 2.5 nm, Fig. 4b. The palladium-copper nanoparticles are semi-spherical with an average particle size of 3 ± 0.46 nm, Fig. 4d. Furthermore, it is observed that the addition of copper to palladium induces a decrement in the particle size.

Besides, to investigate the composition and chemical binding states of the Pd/C and PdCu/C catalyst, X-ray photoelectron spectroscopy (XPS) analysis was accomplished. The elemental quantification of the carbon, sulfur, nitrogen, palladium, copper and oxygen contents are shown in Table 2, and the general spectrum is displayed in Fig. 5a. The composition results of general spectra exhibit a total amount of Pd of ca. 3.7%wt. and 1.8%wt. in Pd/C and PdCu/C catalysts, respectively. Additionally, the high-resolution XPS spectra of the main orbital signals Pd3d ($Pd3d_{5/2}$ and $Pd3d_{3/2}$) were recorded from 333.1 to 345.9 eV and analyzed by deconvolution modeling (Fig. 4b). The model could be fitted with five double spin-orbit components corresponding to Pd in three different kinds of chemical states: metallic Pd, Pd (II) and Pd (IV) [27]. The first contribution of the Pd3d region in Pd/C catalyst is observed in 335.24 and 340.58 ± 0.15 eV for $Pd3d_{5/2}$ and $Pd3d_{3/2}$, respectively. The fitted spectra show a content of 24.8% for metallic palladium, 8.11% for Pd(II) as PdO, and 11.6% of Pd(IV) as PdO_2, 38.4% of Pd(II) as parental species associated to traces of precursor Pd $(C_5H_7O_2)_2$ and 17.1% for Pd-C which is related to the interaction of Pd with the support [28,29]. Respect to the difference in the core-level binding energy between the Pd (0) and Pd (II), the spin-orbit components is 1.34 that are in concordance with the reported in the literature [30]. The formation of PdO_2 species in the surface are linked with the oxidation of Pd species when the samples get in contact with atmospheric air even at low pressures and temperatures [31]. In contrast, the fitted spectra of bi-metallic catalyst (PdCu/C) show the PdO (41.09%) as the main species present in the catalyst and a lower metallic palladium amount (8.2%) and PdO_2 (18.98%); while Pd-C species (19.97%) remains at similar composition. In the case of copper, high-resolution spectra are shown in Fig. 5c. Despite no diffraction peaks for copper oxides in XRD pattern were observed, XPS reveals the presence of this species, probably due to partial oxidation of the PdCu catalyst surface, that are congruent with the major oxygen content obtained by chemical composition analysis in the PdCu/C sample. Nevertheless, it is hard to resolve Cu (0), Cu(OH), $Cu(OH)_2$ and Cu_2O by this deconvolution due to the very close binding energy. Fig. 5c, shows the core level spectrum of Cu 2p, corresponding to $2p_{3/2}$, $2p_{1/2}$ of Cu(0), Cu(II) and shake-up peaks [32]. Here, the fitting peak at 932.5 eV is assigned to Cu_2O, while

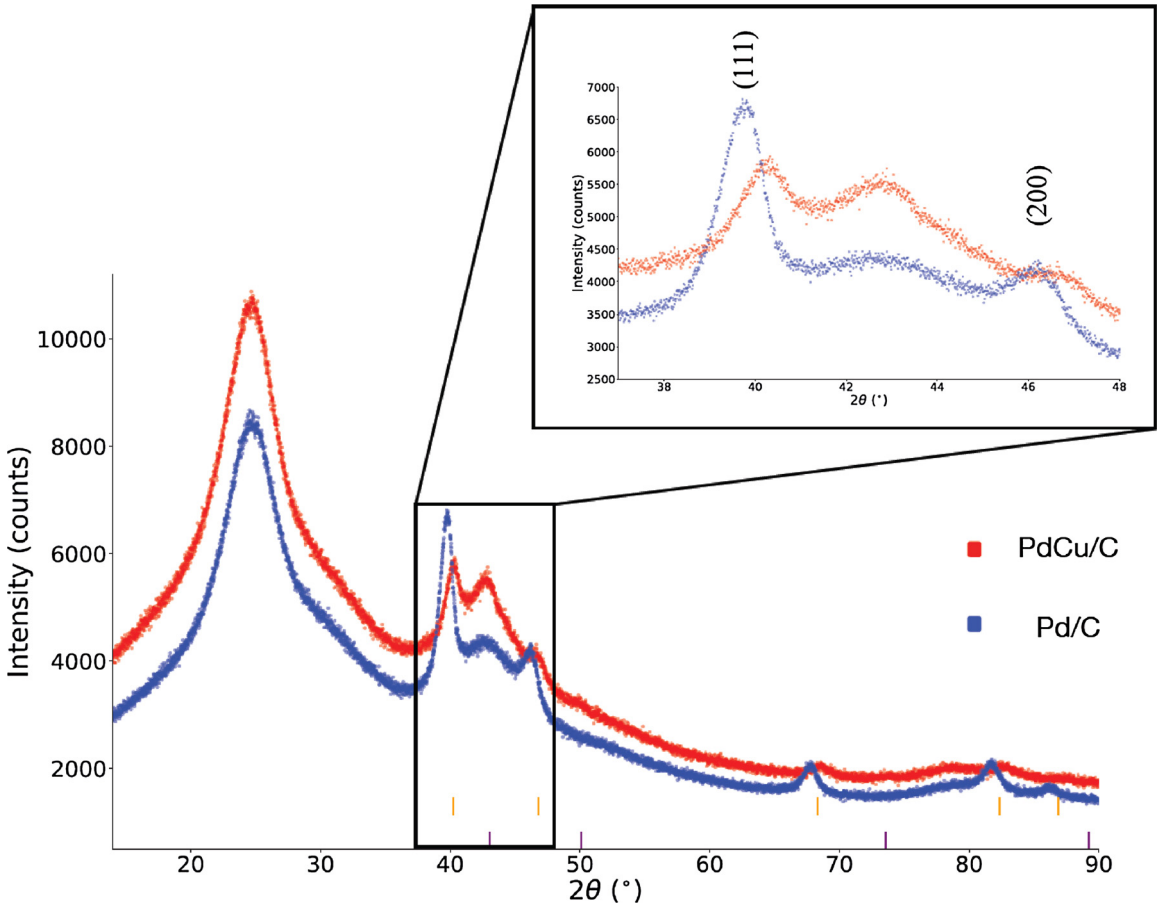

Fig. 3. Comparison of X-ray diffraction patterns of Pd/C and PdCu./C.

Table 1
Crystallite size, lattice constants and phase composition from Rietveld of the as-synthesized Pd/C and PdCu/C.

Catalyst	Phase	RWP	Crystallite size (nm)	Lattice constant "a" (nm)	Cell volume (Å^3)
Pd/C	Pd	2.83	5.64 (6)	3.9038 (5)	59.49 (2)
PdCu/C	PdCu	3.22	4.78 (13)	3.8929 (8)	59.00 (4)
	Cu		1.55 (4)	3.644 (2)	48.39 (8)

the peak at 934.5 eV is ascribed to CuO which is confirmed by the satellite peak at 942.5 eV [33]. Consequently, XPS and XRD analysis confirm the presence of Pd and Cu nanoparticles on the surface of carbon Vulcan support.

3.2. Electrochemical measurements

The electrochemical profiles of the synthesized catalyst Pd/C and PdCu/C on the supporting electrolyte (0.5 M NaOH) at 20mVs^{-1}, are plotted in Fig. 6. In the current–potential (i-E) characteristics, typical hydrogen and hydroxide adsorption/desorption redox process is observed. Initially, anodic process related to oxidized species were detected in both catalysts that confirm the presence of the chemical states found by XPS analysis (Fig. 5). However, these species are removed after the cleaning process (activation): cyclic voltammetry during 50 cycles at 100 mVs^{-1}. The profiles remain unchanged from cycle 35, indicating that the material-interfacial redox-process are stables. Despite no significant differences were marked between both profiles, the hydrogen adsorption observed for the bi-metallic catalyst (between -0.25 and -0.65 V vs RHE) are less evident as a consequence of a lower palladium content (1.8%) and for the addition of copper. That is an important issue for the NO_x electro-reduction due to the competition between this nitrogen-species and hydrogen adsorption that leads to a suppression of hydrogen evolution reaction (HER) at copper interface, as described further in the nitrite and nitrate electro-reduction experiments (Section 3.2.2). It is also possible that the amount of copper in the Pd-based-catalyst (supported in carbon) promotes a different selectivity and conversion toward, for example, molecular nitrogen.

3.2.1. CO stripping analysis

The electrochemical active surface area (ECSA) for Pd and PdCu catalysts was determined by CO-stripping. The electrodes were cleaned-activated using cyclic scans between 0.05 V and 1.2 V at 100 mV s^{-1} in 0.5 M H_2SO_4 until stable current-potential profiles were obtained. Subsequently, the electrochemical CO-stripping current-potential characteristics were obtained by oxidizing the pre-adsorbed CO (CO_{ad}) at a scan rate of 10 mV s^{-1}. The solution was purged with Ar for 20 min to remove dissolved oxygen. The working electrode was polarized at 0.05 V (vs. RHE), then CO was bubbled for 5 min to generate the CO-layer. Thereafter, the solution was purged with Ar for another 20 min. Fig. 7 shows the CVs obtained with CO-adsorbed (curve a) and CO-free (curve b). The associated ECSA was obtained from Eq. (2).

$$ECSA_{CO}(m^2 g_{Pd}^{-1}) = \left[\frac{Q_{CO}(C)}{420\,\mu C\,cm_{Pd}^{-2}\,L_{Pd}\,(mg_{Pd}\,cm^{-2})A_g(cm^2)}\right]10^5 \quad (2)$$

Where Q is the charge of CO desorption-electrooxidation (μC), L_{Pd} is the Pd loading in the working electrode, A_g is the geometric surface area of the glassy carbon electrode [34] and 420 μC cm^{-2} is the charge required to oxidize the monolayer of CO on the Pd catalyst. The ECSA is estimated to be 70.12 m^2 g^{-1} for Pd/C and 90.88 m^2 g^{-1} for PdCu/C

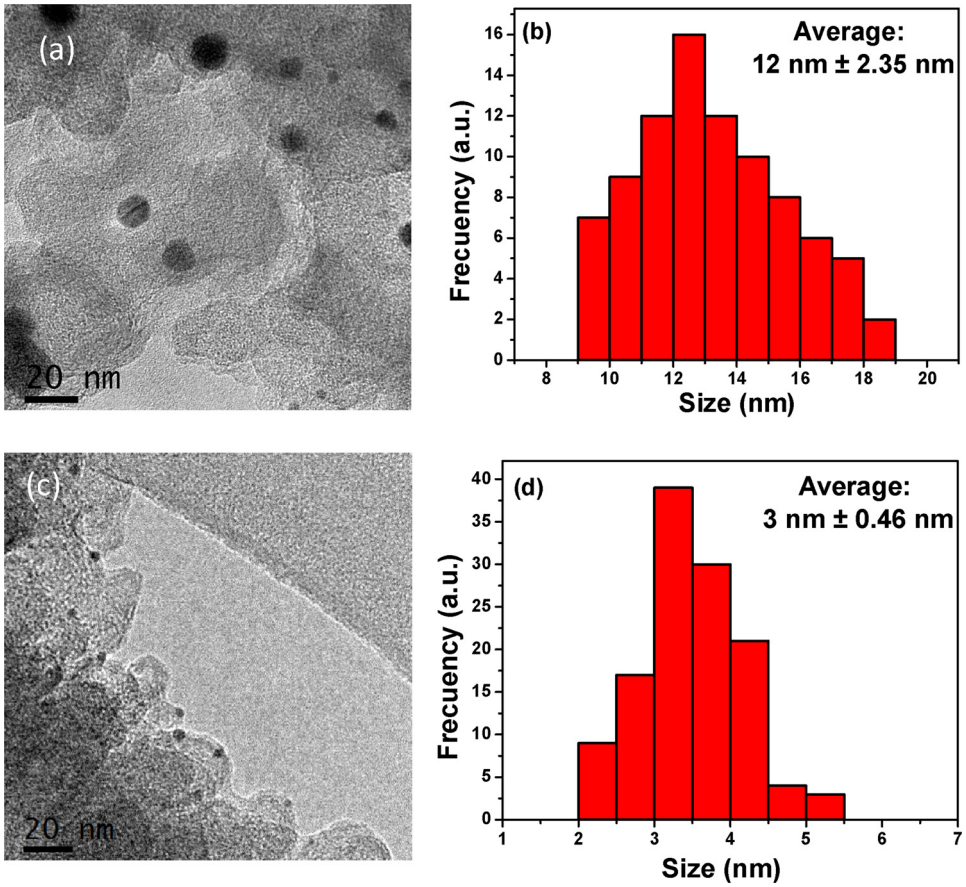

Fig. 4. TEM micrographs obtained for Pd/C (a) and PdCu/C (c), and the respective particle-size distribution (b, d).

Table 2
Elemental quantification and binding energy obtained from XPS survey spectra of the Pd and PdCu/C catalyst.

Catalyst		C1s	O1s	Pd3d	Cu2p	N1s	S2p
Pd/C	[wt.%]	86.2	6.9	3.7	–	2.0	1.2
	Binding energy (B.E)	285.025	532.2141	336.083	–	399.85	163.08
PdCu	[wt.%]	81.9	9.4	1.8	1.9	4.1	0.9
	Binding energy (B.E)	285.071	532.077	338.075	934.98	400.05	164.27

(Table 3). The larger ECSA value obtained for the bi-metallic catalyst is associated with the smaller crystallite size and a better distribution of the Pd and Cu nanoparticles on the support, as observed previously by XRD and TEM analysis. This is also associated with a high number of active sites available for the reaction and is an indicator of the improvement in the electrocatalytic performance when copper is added [35]; even though the metal loading is 3.7%wt for the Pd on Pd/C (Fig. 5a), and 1.8%wt for Pd on PdCu/C (Fig. 5b), as was determined by XPS analysis.

3.2.2. Nitrate (NO_3^-) and nitrite (NO_{2-}) ions electrochemical reduction

As previously mentioned, the NO_x species encompasses a mixture of different nitrogen oxidation states. Consequently, the aim of this work is conducted to the study of electrochemical reduction of these pollutants. To have an overview of the general electrochemical reduction of this species, experiments with different concentrations of NO_3^- and NO_2- and blank NaOH saturated solution with NO or NO_2 were performed using cyclic voltammetry technique at a scan rate of 20 mVs^{-1} at 25 °C.

The i-E profiles of the electro-reduction reaction of NO_3^- using NaOH (0.5 M) as supporting electrolyte in a potential interval from 0.6 to −0.8 V vs RHE at 20 mV/s are plotted in Fig. 8(a, b) for Pd/C and PdCu/C electrocatalyst, respectively. In the graphs, the arrow indicates the starting potential. It is observed that the current density increases as a function of concentration, having the major reduction current at 1.0 M. Nevertheless, PdCu/C exhibit a better performance for the nitrate electro-reduction of ca. 6.0 times higher with respect to Pd/C for the same concentration.

According to the literature, for the electrochemical reduction of nitrate (NO_3^-), an initial adsorption step of this specie onto the catalyst surface is needed. Consequently, the reduction of NO_3- encompass an Electrochemical-Chemical- Electrochemical (ECE) reaction sequence. The first step is an electron transfer mechanism (E), and as a second step a homogeneous chemical reaction (C), obtaining a more easily reducible species that leads to a second electron charge transfer (E) as a third step [36,37,47]. These steps allow the rupture of the nitrogen–oxygen (N–O) bond, giving the formation of nitrite (NO_2^-) ions as the main intermediate before its complete reduction. That is linked with the significant difference in the current density observed when nitrate concentration was modified. Initial steps in the reaction mechanism in the alkaline-supporting-environment are indicated in Eqs. (3,4).

$$NO_3^- \rightarrow NO_{3ads}^- \quad (3)$$

$$NO_{3ads}^- + H_2O + 2e^- \rightarrow NO_{2ads}^- + 2OH^- \quad (4)$$

This reaction is a mass-transfer limited process: concentration affects the species-diffusion from the bulk-solution towards reactive surface. This is in concordance with our experiments with respect to the concentration of NO_3^- and faradic current from ca. -0.5 to -0.7 V/RHE,

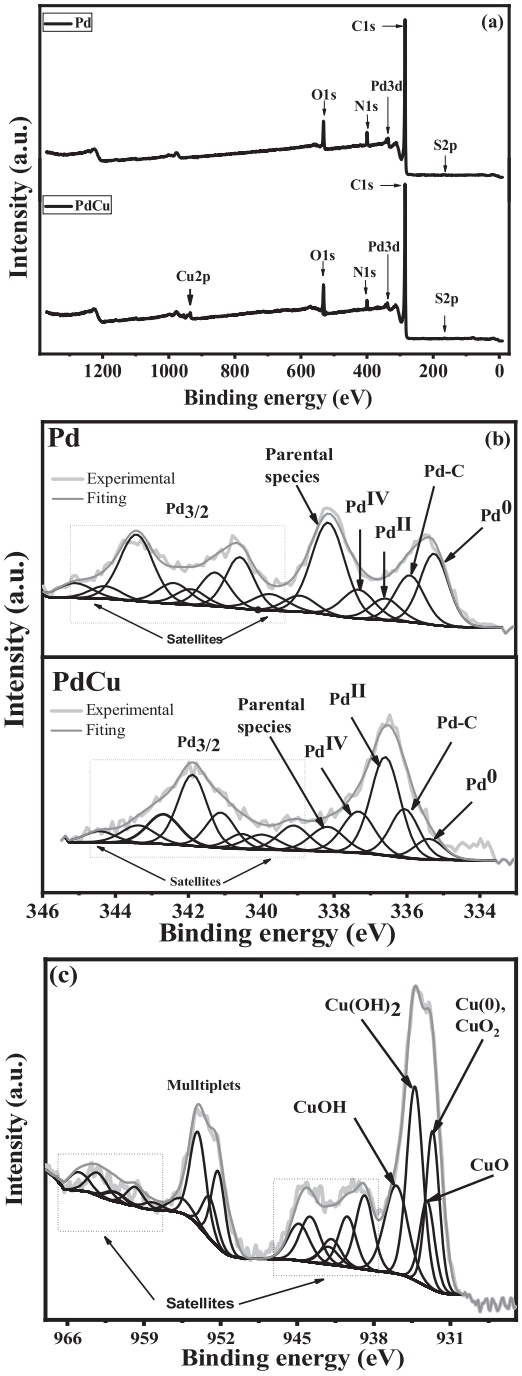

Fig. 5. (a) General XPS spectra of Pd and PdCu catalyst, (b) high-resolution spectra and deconvolution for Pd 3d in the $3d_{5/2}$ and $3d_{3/2}$ orbitals and (c) high-resolution spectra and deconvolution for Cu in the Cu2p in the $2p_{3/2}$ and $2p_{1/2}$ orbitals.

while the values for HER are quite similar for both catalysts (ca. 320 μA/cm^2). The same methodology was used for experiments as a function of nitrite concentration; the potential was fixed at −0.9 V as the HER is shifted toward more negative potentials, due to the presence of copper in the catalyst, Fig. 9(a, b). Similar behavior was observed during the electro-reduction process. However, two main differences were noted i) a significant enhancement in current density for nitrites electrochemical reduction was obtained for both catalysts, revealing a higher catalytic reduction process even at low concentration (0.001 M) with a better performance for the PdCu/C sample (of ca. 6.0 times higher) with respect to nitrate-ions electro-reduction; and ii) a notable

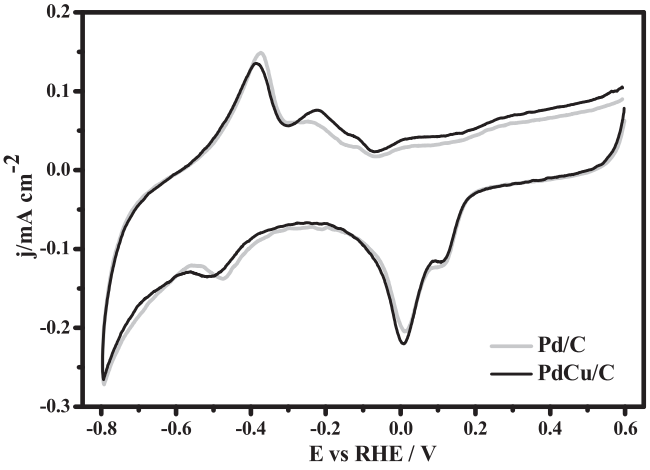

Fig. 6. i–E profile for (a) Pd/C and (b) PdCu/C in NaOH (0.5 M) at scan rate of 20 mVs^{-1}.

onset to more negative potentials for the HER (dashed line in Fig. 9b) that might be linked with a slight local-pH variation and/or mass transport limitations as concentration increases.

In order to understand the complexity of the reactions in study, Fig. 10 displays the profiles corresponding to peak potential (a, d) and peak current (b, e) with respect to concentration for both materials (Pd/C and PdCu/C) evaluated in solutions containing NO_3^- and NO_2- ions. It is interesting to observe a displacement of E_p to more negative potentials as the concentration increases, suggesting that the electron transfer is a process limited by diffusion. In addition, the peak current (i_p) also increases in a linear form with the concentration of nitrites (Fig. 10e). Nevertheless, for the reduction of NO_3- the profiles present two slopes related to a combination of charge-transfer and mass-transfer process (Fig. 10a–c) [38,39]. Whereas, the plots of log I vs log C obtained at -0.56 V and -0.54 V/RHE for NO_3^- and NO_2- respectively (c, f) also displays charge/mass process transfer and it is independent of the catalyst in turn. Therefore, nitrite ions-interfacial interaction and their reduction is a key factor for the selectivity and complete formation of nitrogen (N_2). In this context, the nitrite reaction mechanism in alkaline-supporting electrolyte would be described from Eqs. (5–7) [36], without the formation of N_2O and NH_2OH (Section 3.3).

$$NO_2^- \rightarrow NO_{2ads}^- \quad (5)$$

$$NO_{2ads}^- + H_2O + e^- \rightarrow NO_{ads} + 2OH^- \quad (6)$$

$$NO_{ads} \rightarrow N_2,\ N_2O,\ N_2H_4,\ NH_2OH,\ NH_3 \quad (7)$$

In a general form, a proposed reaction pathway at the interface of Pd and Cu could be represented according to Eqs. (8–12), with HER at more cathodic potentials, Eq. (10). During electrochemical reduction of nitrate in aqueous media, water is reduced to a stable specie (H_{ads}) which is adsorbed on the palladium surface (PdH_{ads}) (Eqs. 8) [15]. Thus, Pd supply the protons required to the hydrogenation of adsorbed NO_3^- given rise to the N-H adsorbed species, and subsequent reduction toward Nitrogen (N_2), hydrazine (N_2H_4) and ammonia (NH_3) Eq. (9), as observed with DEMS.

$$Pd + H_2O + e^- \rightarrow PdH_{ads} + OH^- \quad (8)$$

$$NO_{2,ads}^- + PdH_{ads} \rightarrow \ldots \rightarrow Pd + N_2,\ N_2H_4,\ NH_3 \quad (9)$$

$$4H_2O + 4e^- \rightarrow 2H_2 + 4\,OH^- \quad (10)$$

Whereas, the use of copper as second-assigned catalyst, favors the kinetic-reduction process of nitrate to nitrite (as reaction-determined step) for the generation of nitrogen and ammonia [9–11]. In this process, the Cu surface are oxidized to Cu_2O_{ads} by reducing nitrate ions (Eq. 11). In a parallel reaction, the presence of PdH_{ads} promotes the

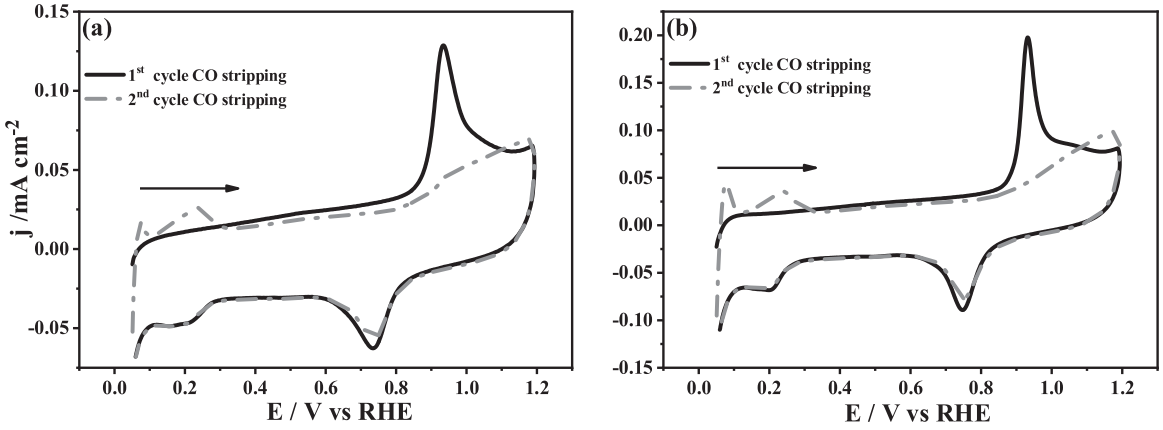

Fig. 7. Electrochemical active surface area (ECSA) of Pd sites in (a) Pd/C and (b) PdCu/C catalysts determined by CO-stripping (black line), 0.5 M H_2SO_4 recorded at 10 mVs^{-1}.

Table 3
Charge and ECSA obtained by CO stripping.

Catalyst	Q[=] μC	ECSA [=]m^2/g
Pd/C	178.36	71.259
PdCu/C	123.72	98.844

"spill" or migration of hydrogen to the Cu surface (PdH_{spill}) allowing the in-situ reduction of these metal and promoting the regeneration of the catalytic surface as described in equation (12) [12,16].

$$NO_3^- + 2\ Cu + e^- \rightarrow Cu_2O_{ads} + NO_{2,ads}^- \quad (11)$$

$$2Cu_2O_{ads} + 2PdH_{spill} \rightarrow 2\ Pd + 4\ Cu + 2OH^- \quad (12)$$

In our case, the coupling with DEMS verifies the presence of nitrogen-formed species during cathodic polarization at the Pd-Cu/C interface. Interestingly, at the Pd/C surface no nitrogen-species mass-signal were observed, see Section 3.3.

3.2.3. Nitric oxide ($NO_{(g)}$) and nitrogen dioxide ($NO_{2(g)}$) electrochemical reduction

Following with this analysis, from the information of the i-E profiles obtained at nitrate and nitrite electrochemical-reduction zone, linear voltammetry technique was performed from −0.2 to −0.8 V (vs RHE) to obtain the i-E profiles during the electrochemical reduction-reaction of nitric oxide (NO) and nitrogen dioxide (NO_2), which are displayed in Fig. 11 for both catalysts in study. For such an approach, the solution was saturated with the gas in turn during 20 min at a flow rate of 11.5 mL/min, in a solution of 0.5 M NaOH (previously saturated with Ar to remove dissolved oxygen) until the open circuit potential (OCP) and the pH remained quasi-constant and obtaining a gas concentration of ca. 600 ppm. The NO employed was a commercial mixture of 90% Ar and 10% NO (INFRA); whereas the NO_2 was synthesized according to the procedure described in Section 2 (see also Fig. 1).

At his conditions, during saturation of NO in alkaline solution, a hydrolysis process to form NO_2 and HNO_2 take place at concentrations below 2000 ppm, Eqs. (13,14). Also, it has been found that the overall-reduction process is controlled by these species [41,43].

$$2\,NO_{(g)} + OH^- \rightarrow 2\,NO_{2\,(aq)} \quad (13)$$

$$NO_{(aq)} + NO_{2(aq)} + H_2O \leftrightarrow 2HNO_{2(g)} \quad (14)$$

As shown in the reaction pathway, when nitrogen oxides interact in the alkaline solution, the nitrite (NO_2^-) and nitrate (NO_3^-) ions are formed chemically (Eq. 15). Also, HNO_2 is quickly ionized and then neutralized by the OH^-, promoting the formation of NO_2^- ions (Eq. 16) [36,41,43]. This is in concordance with the higher electrochemical activity observed in our experiments, when the NO is present in the solution, see below.

$$2\,NO_{2(aq)} + 2OH^-_{(aq)} + H_2O \rightarrow NO^-_{3(aq)} + NO^-_{2(aq)} + H_2O \quad (15)$$

$$HNO_{2(g)} + OH^-_{(aq)} \rightarrow NO^-_{2(aq)} + H_2O \quad (16)$$

The i-E profiles obtained from the electrochemical reduction reaction process for both catalysts exhibit a similar profile, with a slight shift in the peak potential (E_p) for the PdCu/C catalyst. In addition, a more intense current reduction-peak is observed in comparison to Pd/C,

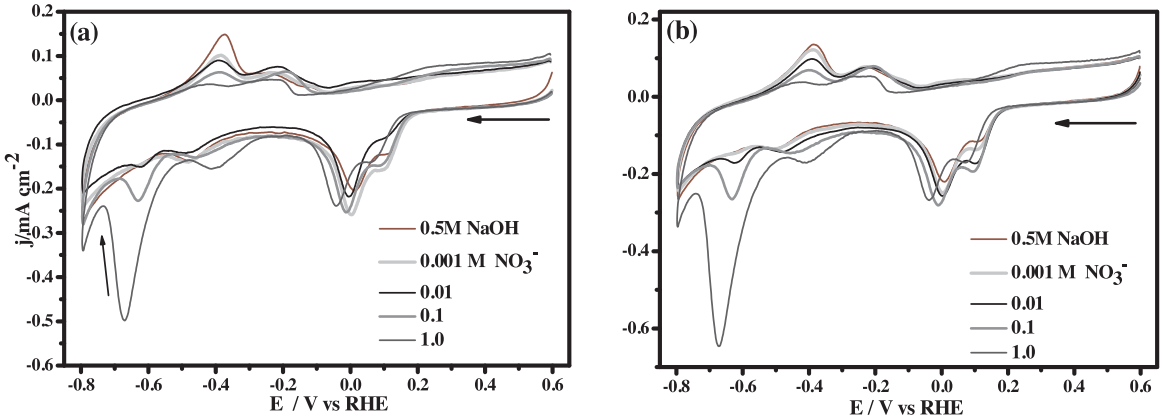

Fig. 8. i–E profile for (a) Pd/C and (b) PdCu/C catalysts at different nitrate concentration of NO_3^-, using NaOH (0.5 M) as supporting electrolyte at scan rate 20 mVs^{-1}.

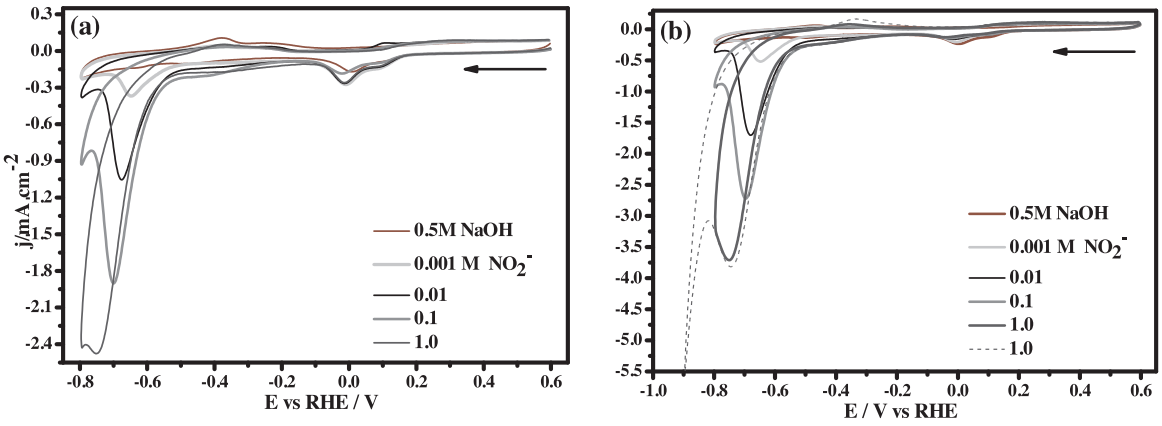

Fig. 9. i–E profile for (a) Pd/C and (b) PdCu/C catalysts at different nitrite concentration of NO_2^-, using NaOH (0.5 M) as supporting electrolyte at scan rate of 20 mVs^{-1}. The dotted lines correspond to a potential of -0.9 at the same concentration, for more details refer to the experimental section.

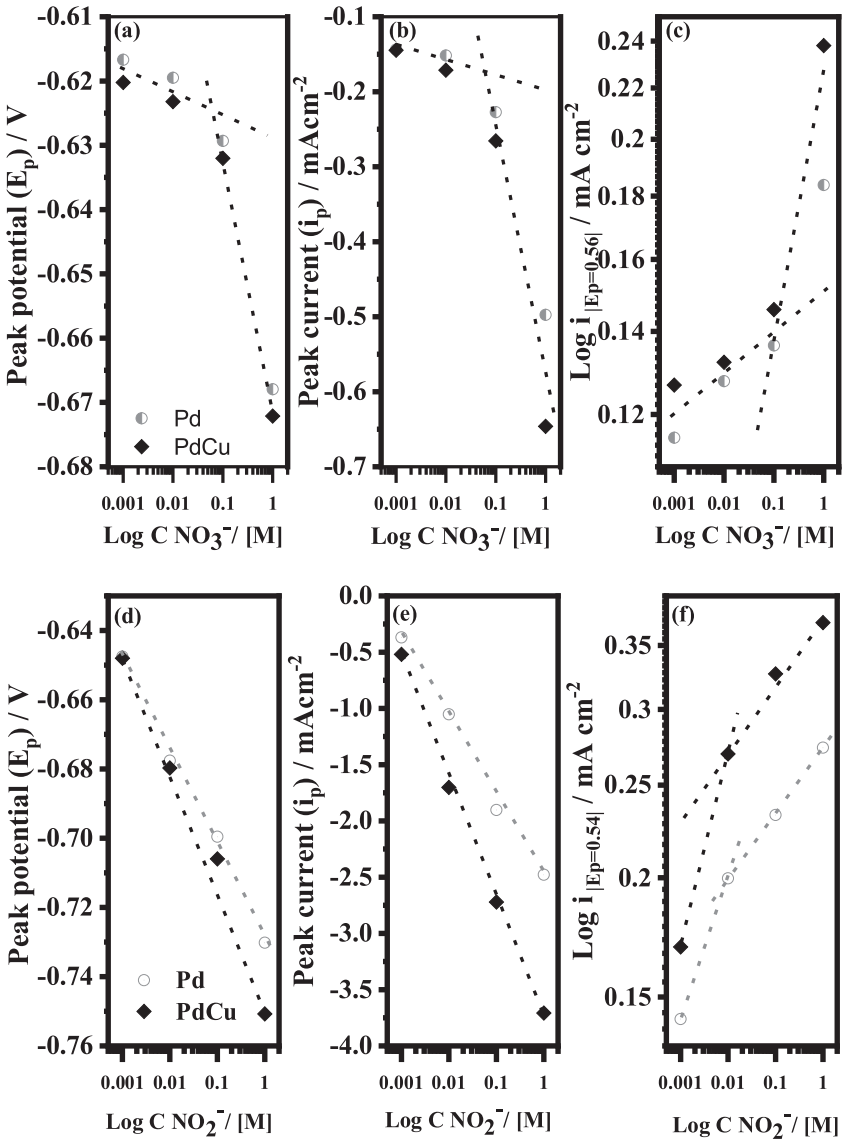

Fig. 10. Peak potential (a,d), peak current (b,e) and log of current (c,f) at a constant potential (0.54 and 0.56 for NO_2^- and NO_3^-, respectively) as a function of concentration for (a) Pd/C and (b) PdCu/C.

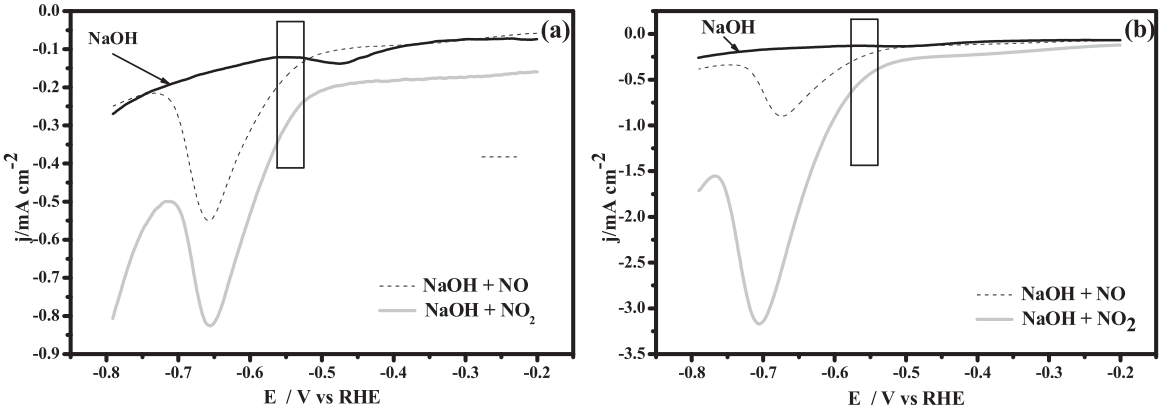

Fig. 11. i–E profile for (a) Pd/C and (b) PdCu/C catalysts exposed to NO and NO_2. Scan rate of 20 mVs^{-1}.

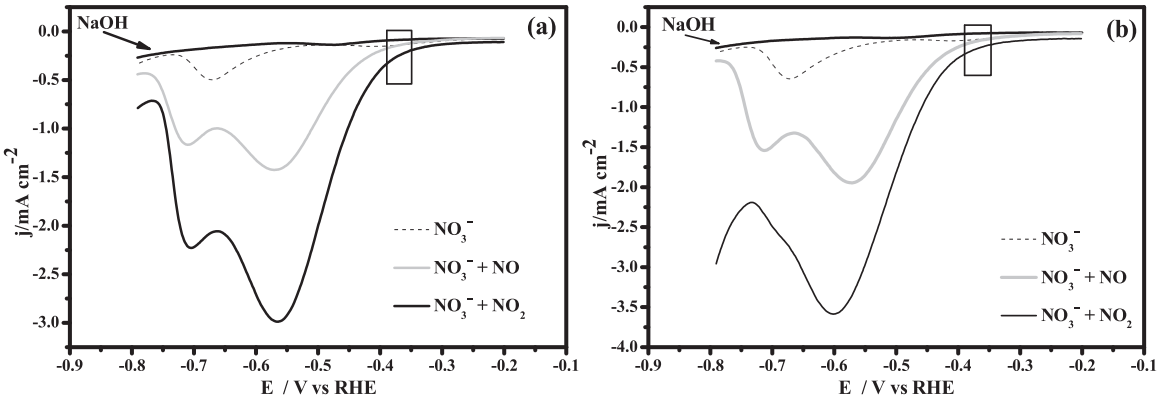

Fig. 12. i–E profile of electro-reduction mixtures of NO_3^- + NO and NO_{3-} + NO_2 for (a) Pd/C and (b) PdCu/C catalysts, at scan rate of 20 mVs^{-1}.

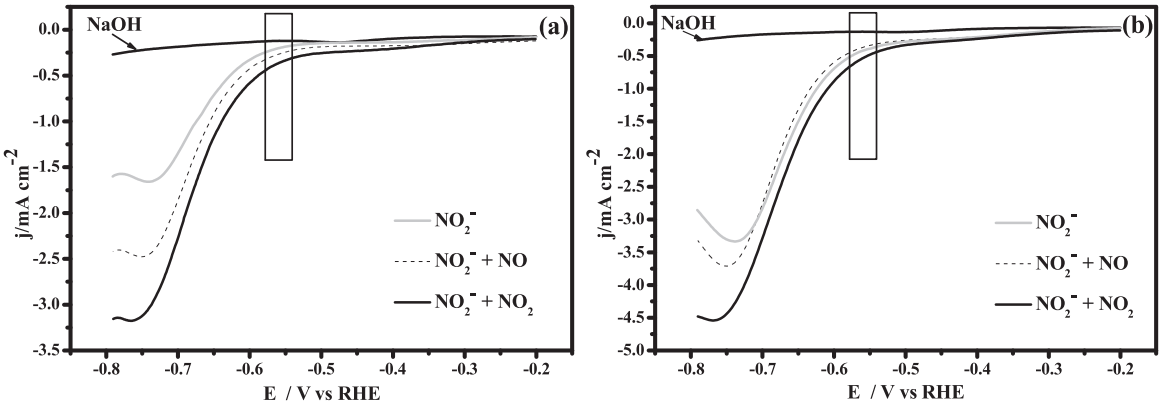

Fig. 13. i–E profile of electro-reduction mixtures of NO_2^- + NO and NO_{2-} + NO_2 for (a) Pd/C and (b) PdCu/C catalysts, at scan rate of 20 mVs^{-1}.

ascribed to the synergic effect between palladium and copper on the catalyst surface.

3.2.4. Nitric oxide (NO) and nitrogen dioxide (NO_2) interaction at NO_3^- and NO_{2-} solutions

For this case of study, the i-E profile for each gas (NO and NO_2) in the supporting electrolyte (NaOH) was obtained and from this information, the electrochemical response of the mixture between the gases and the ions (NO_3^- and NO_{2-}) is discussed. For such an approach, the concentration with the highest catalytic activity was selected (i.e. 1.0 M) in the alkaline environment (0.5 M NaOH) saturated with NO or NO_2 and compared with solutions free of nitrogen species. It is worth to mention that a slight variation of pH (from 13.2 to 12.8) was observed during saturation with NO_2; whereas a quasi-constant pH (ca. 13.4) was observed during saturation with NO. The process associated with the reduction of these gases was recorded at the same potential interval than those obtained during the reduction of NO_3^- and NO_{2-}ions. The i-E profiles generated for the different combinations with NO and NO_2 keeping concentration of NO_3^- constant (1.0 M) for Pd/C and PdCu/C are shown in Fig. 12, whereas similar experiments using NO_2^- (1.0 M) as supporting electrolyte are plotted in Fig. 13. It is important to note that when NO is added to NO_3^- solutions, the profiles of reduction current exhibit a considerably increment and a second reduction peak appearing at potential of ca.-0.4 V vs RHE with a maximum peak-current observed at −0.57 V vs RHE that would be linked to the hydrolysis of NO in the bulk solution. Since this compound generates simultaneous process as dissolution, diffusion and reaction of different species, being dissolved nitrite the main product in alkaline solutions. Conversely, in NO_2^- solutions it was observed a decrease in the reduction current that might be associated with i) an electrode surface saturation due to

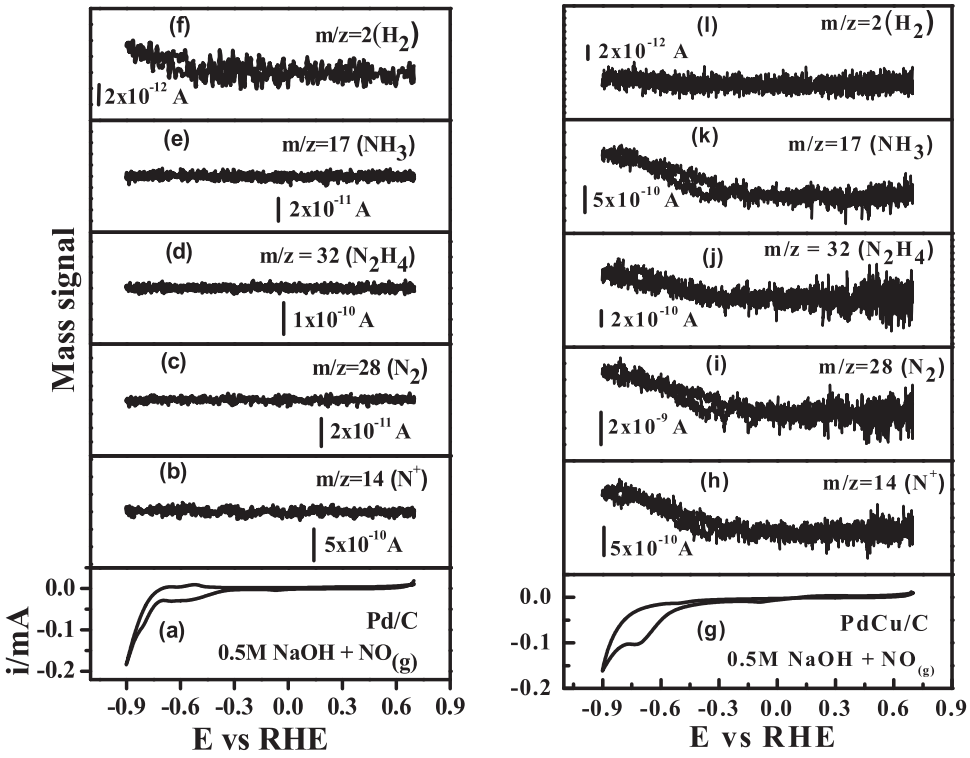

Fig. 14. i-E characteristic obtained for (a) Pd/C and (g) PdCu/C in the electro-reduction of NO in 0.5 M NaOH; and ion current (mass signal) versus potential obtained using DEMS for (b, h) N^+, (c, i) N_2, (d, j) N_2H_4, (e, k) NH_3 and (f, l) H_2. Scan rate of 2 mVs^{-1}.

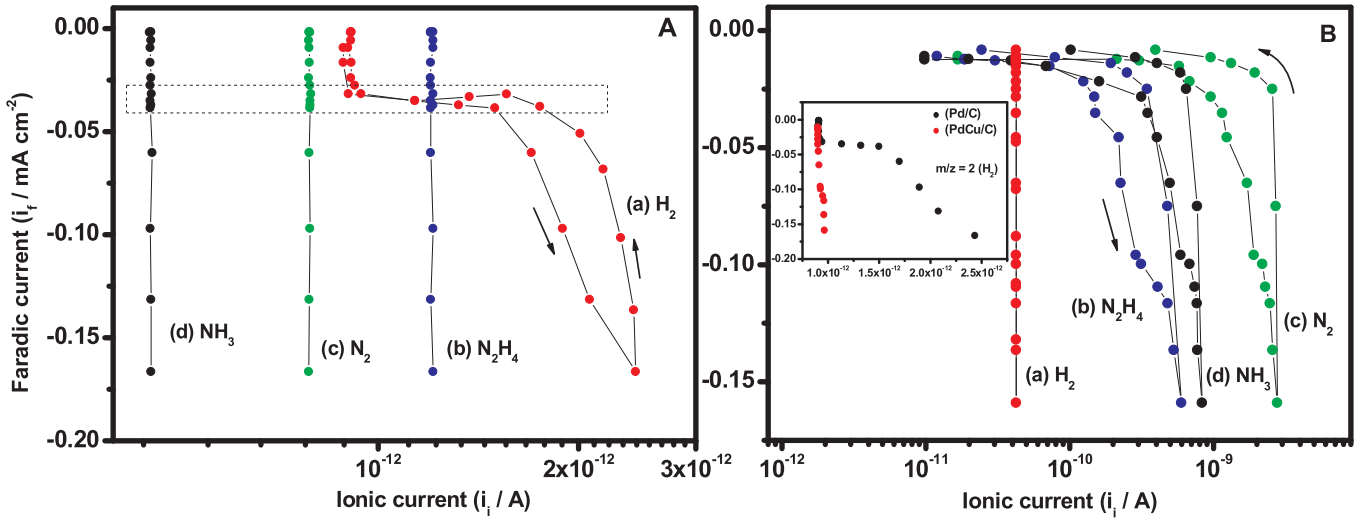

Fig. 15. Faradic-current (i_f) versus ionic-current (log i_i) profiles (one cycle) obtained from potentiostatic-current and mass-intensity data ((a) hydrogen, (b) hydrizine, (c) nitrogen, and (d) ammonia) for Pd (A) and PdCu/C (B) catalyst in a saturated NO solution of NaOH 0.5 M. Inset: (i_f) versus (log i_i) in the Hydrogen Evolution Reaction (HER) domain, only the negative-going scan is plotted. The scan rate was 2 mV/s.

reduced species that act as a steric hindrance inhibiting the diffusion of species and ii) poisoning due to adsorption of nitrogen species on the catalyst surface. In the same way, mixtures of nitrogen dioxide were development with the ion solutions (Fig. 13). In these experiments, an increase in reduction current was observed in all cases. However, when the NO is saturated in the 1.0 M of NO_3^- or NO_2- solution, only one peak was observed with a slight process at ca. −0.7 V vs RHE, that would be associated with a second peak related to the competition process involved in this complex mixture; since in alkaline solutions hydrolysis reactions of NO_2 can generated HNO_2 and N_2O_4 which are the rate determined steps. In the case of the nitrite and NO_2, a similar trend was observed when the potential was shifted to −0.9 V. This change in the potential is due to the on-set in the hydrogen evolution observed in the i-E profile. Despite both reduction processes are in the same order of magnitude, the clearest reduction of NO and NO_2 processes are exhibit when NO_2^- ions are present in the solutions. In agreement with the literature [40,41] nitric oxide (NO) interacts in the supporting electrolyte in turn to form NO_2, N_2O_4 or HNO_2 species, causing the decrement in NO content. In this sense, the overall absorption rate of NO_2 is higher respect to NO; resulting in a poor selectivity due to an equimolar formation of nitrites and nitrates species. To summarize, the reduction process might be linked with i) the interaction-reduction of an interfacial mono-layer generated at the electrode during saturation-polarization with the gas in turn; and ii) the

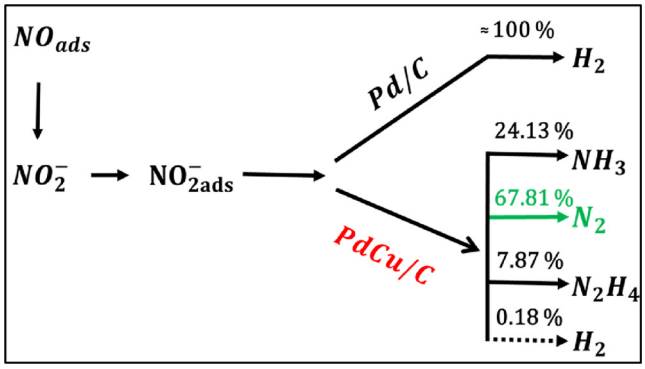

Scheme 1. A proposed pathway for the reduction of NO at PdCu/C and Pd/C catalysts from DEMS studies at scan rate of 2 mV/s.

reduction of formed species (NO_3^- and NO_{2-}) during gas-hydrolysis, as reported employing different metals in the nitrate reduction process [42,43]. The Tafel slopes for the electrochemical reduction of NO_x mixtures (NO, NO_2, NO_3-, NO_2) was obtained on the initial adsorption potential of ca. −0.35 and −0.52 V (vs RHE) from Figs. 11, 12 respectively. Within experimental error, the mechanism is very similar on both catalysts as was observed in the i-E profiles. The calculated Tafel slopes linked to NO and NO_2 electro-reduction (in NaOH base electrolyte) were −165 and −291 mV dec^{-1}, respectively. These results are in agreement with those obtained at nitrate and nitrite solutions evaluated in the same potential window. Whereas for the mixtures the Tafel slopes were −386 and −617 mV dec^{-1} for NO_3- + NO and NO_2- + NO_2, respectively. Consequently, NO_x electro-reduction takes place with an Electrochemical-Chemical-Electrochemical (ECE) reaction sequence, as described above in the Eqs. (3–16).

3.3. Differential electrochemical mass spectrometry (DEMS)

The analysis of generated species was carried out in a 0.5 M NaOH solution saturated with NO (previously purged with Ar for 10 min). During saturation of NO into the cell-DEMS, mass signals related with such gas were monitored, for this case 20 min of saturation. Fig. 14 shows the Faradic (i-E) and the ionic (mass-signal) current-potential profiles corresponding to the reduction of nitrogen oxide-adsorbed species onto Pd (a) and PdCu (g) catalysts obtained when the electrochemical cell is coupled with the DEMS system. Both experiments were developed independently in NO-purged 0.5 M NaOH solution. The mass signals magnitude linked with NO (m/z = 30, 14, 32) were constant as well as the OCP. On the other hand, the mass signals corresponding to N^+ (m/z = 14), N_2 (m/z = 28), N_2H_4(m/z = 32), NH_3 (m/z = 17) and H_2 (m/z = 2) were recorded during cyclic voltammetry experiments from 0.7 to -0.9 V/RHE at a scan rate of 2 mVs^{-1} (Fig. 14, b–f and h–l). For example, in Fig. 14(a) the faradic current-versus-potential characteristic for reduction using Pd/C catalyst is plotted. For this case two processes are observed: the reduction of species at a potential of ca. −0.6 V and the hydrogen evolution reaction at ca. −0.8 V/RHE. These results are consistent with the electrochemical response obtained using DEMS, in Fig. 14(b–f) no reduction of nitrate species signals are obtained, and only the H_2 signal was observed at ca. −0.8 V/RHE, which suggests that this system leads to hydrogen evolution.

Whereas, the obtained characteristic of PdCu/C during NO reduction reaction is shown in Fig. 14(g). In contrast with the mono-metallic catalyst, it was observed an increment of faradic-reduction current of ca. 3 times higher. This variation could be related to the catalytic effect of the copper present in the catalyst. Also, mass signals measurements reveal the generation of ionic current assigned to N^+ (m/z = 14), N_2 (m/z = 28), N_2H_4 (m/z = 32), NH_3 (m/z = 17) and H_2 (m/z = 2) (Fig. 14, h–l). It is important to note that nitrogen (N_2) ionic current is one order of magnitude higher than the recorded from N_2H_4 and NH_3 (see also Fig. 15B) suggesting that the bimetallic catalyst modulated the selectivity and conversion toward molecular nitrogen; this conversion is close to 100% with respect to the monometallic Pd/C (zone marked with a rectangle in Fig. 15A) at the experimental condition in the DEMS reactor. In addition, the detection of N^+ (m/z = 14, Fig. 14h) confirms the formation of molecular nitrogen N_2 (m/z = 28). These generated-species during polarization are in good agreement with those proposed in other works using copper in both neutral and alkaline media [22,44]. In this context, from the Frost diagram, it is known that hydrazine and ammonia can be formed in alkaline media, being one of the most reduced oxidation states of nitrogen (-II) and (-III), respectively [36]. This species has also been observed in a based copper system [18,45,46]. Also note that the hydrogen generation is less marked in the bi-metallic catalyst (Fig. 14-l and inset in Fig. 15B (normalized for comparison)) associated to the competition with the electrochemical reduction of NO_3^- that would consume the circulated electrons, inhibiting the hydrogen evolution reaction (HER) toward more cathodic potential (inset). Therefore, employing the synthesized PdCu/C catalyst, a possible sequence of the products generated from the electrochemical reduction of NO_x (hydrolyzed into NO_2^-) are showed in Eqs. (17–19), Scheme 1 and Fig. 15B.

$$NO_2^- + 6e^- + 5H_2O \rightarrow NH_3 + 7\,OH^- \quad (17)$$

$$2NO_2^- + 10e^- + 8H_2O \rightarrow N_2H_4 + 12\,OH^- \quad (18)$$

$$2NO_2^- + 6e^- + 4H_2O \rightarrow N_2 + 8\,OH^- \quad (19)$$

Then this difference observed could be attributed to the selectivity and intrinsic nature of the materials in study. The conversion of NO to nitrogen-based species was calculated using the relationship obtained from ionic-current (i_i) to potentiostatic-faradic (i_f) signal (Fig. 15B) As can be deduced from this Figure, the ionic current for N_2 is notable during the faradic process, followed by NH_3 and hydrazine. Interestingly, no marked variation in the ionic current for hydrogen was observed (m/z = 2, curve (a), Fig. 15B) indication that the HER is delayed or suppressed during the electrochemical generation of nitrate species. This is also verified with respect to the assigned ionic-current (i_i) from HER at Pd/C electrode, see Fig. 15A and inset in Fig. 15B.

These results are promising for the improvement of electrocatalytic systems which could diminish the use of noble metals as palladium. In this context, the surface state of the material in turn could be electrochemically re-activated/re-used by applying a bias-potential determined by its intrinsic nature and surrounding-interfacial pH.

4. Conclusions

A detailed chemical, structural and electrochemical analysis was carried out in order to understand the interaction of NO_x species (NO_3^-, NO_{2-}, NO and NO_2) at the surface of synthesized palladium and palladium-copper nanoparticles supported on carbon Vulcan. XRD allowed the phase identification and TEM analysis showed the creation of a well-dispersed Pd and PdCu nanoparticles (with a ca. 3–12 nm in diameter) on the carbon Vulcan support. Besides, XPS revealed a total amount of 3.7%wt of palladium at the mono-metallic electrode; whereas 1.8%wt. of palladium was calculated at the bi-metallic catalysts. On the other hand, electrochemical measurements exhibited process linked to the reduction of NO_x species, even in a saturated solution with NO and/or NO_2; and then the HER is suppressed as protons are consumed during the reduction of NO_x at moderated potentials (from −0.5 to −0.7 V/RHE). These interactions were also confirmed during experiments as a function of NO_3^-/NO_{2-} concentration. PdCu/C catalyst exhibited a significant increase (ca. 6 times higher) in the NO_2-reduction reaction. In addition, DEMS experiments (i_i versus E and i_f versus i_i) confirm that the bi-metallic catalyst can reduce the NO-formed species mainly to nitrogen, hydrazine and ammonia which could be further purified and re-used. Therefore, the understanding and

control of these parameters could lead to an improvement in electrochemical reduction of NO_x pollutants employing materials with a low noble-metal amount and less expensive metals such as copper, allowing the production of low-cost electrocatalysts.

Declaration of Competing Interest

The authors declare that they have no known competing financial interests or personal relationships that could have appeared to influence the work reported in this paper.

Acknowledgments

The authors thank the financial support giving through the projects ESIQIE-SIP-IPN-20180430, 20195212 as well as COFAA and CONACyT (projects DEMS 160333, 247208 and 157613). JSH and CRSR acknowledge the financial support from CONACyT within the doctoral fellowship. AM-R appreciates Prof. N. Alonso-Vante (Poitiers University, France).

References

[1] J.N. Armor, Environmental catalysis, Appl. Catal. B Environ. 1 (1992) 221–256.
[2] F.R. Greer, M. Shannon, Infant methemoglobinemia: the role of dietary nitrate in food and water, Pediatrics 116 (2005) 784–786, https://doi.org/10.1542/peds.2005-1497.
[3] G. Centi, P. Ciambelli, S. Perathoner, P. Russo, Environmental catalysis: trends and outlook, Catal. Today 75 (2002) 3–15, https://doi.org/10.1016/S0920-5861(02)00037-8.
[4] A.M. Fan, V.E. Steinberg, Health implications of nitrate and nitrite in drinking water: an update on methemoglobinemia occurrence and reproductive and developmental toxicity, Regul. Toxicol. Pharmacol. 23 (1996) 35–43, https://doi.org/10.1006/rtph.1996.0006.
[5] K.A. Karanasios, I.A. Vasiliadou, S. Pavlou, D.V. Vayenas, Hydrogenotrophic denitrification of potable water: a review, J. Hazard. Mater. 180 (2010) 20–37, https://doi.org/10.1016/j.jhazmat.2010.04.090.
[6] L. Castoldi, L. Lietti, I. Nova, R. Matarrese, P. Forzatti, F. Vindigni, S. Morandi, F. Prinetto, G. Ghiotti, Alkaline- and alkaline-earth oxides based lean NO_x traps: effect of the storage component on the catalytic reactivity, Chem. Eng. J. 161 (2010) 416–423, https://doi.org/10.1016/j.cej.2009.10.065.
[7] I. Nova, L. Lietti, P. Forzatti, Mechanistic aspects of the reduction of stored NO_x over Pt-Ba/Al_2O_3 lean NO_x trap systems, Catal. Today 136 (2008) 128–135, https://doi.org/10.1016/j.cattod.2008.01.006.
[8] S.W. Bae, S.A. Roh, S.D. Kim, NO removal by reducing agents and additives in the selective non-catalytic reduction (SNCR) process, Chemosphere 65 (2006) 170–175, https://doi.org/10.1016/j.chemosphere.2006.02.040.
[9] J.A. Caton, Z. Xia, The selective non-catalytic removal (SNCR) of nitric oxides from engine exhaust streams: comparison of three processes, J. Eng. Gas Turbines Power 126 (2004) 234–240, https://doi.org/10.1115/1.1688366.
[10] M. Tayyeb Javed, N. Irfan, B.M. Gibbs, Control of combustion-generated nitrogen oxides by selective non-catalytic reduction, J. Environ. Manage. 83 (2007) 251–289, https://doi.org/10.1016/j.jenvman.2006.03.006.
[11] J. Van Caneghem, J. De Greef, C. Block, C. Vandecasteele, NO_x reduction in waste incinerators by selective catalytic reduction (SCR) instead of selective non catalytic reduction (SNCR) compared from a life cycle perspective: a case study, J. Clean. Prod. 112 (2016) 4452–4460, https://doi.org/10.1016/j.jclepro.2015.08.068.
[12] S. Roy, M.S. Hegde, G. Madras, Catalysis for NO_x abatement, Appl. Energy 86 (2009) 2283–2297, https://doi.org/10.1016/j.apenergy.2009.03.022.
[13] M. Paidar, I. Roušar, K. Bouzek, Electrochemical removal of nitrate ions in waste solutions after regeneration of ion exchange columns, J. Appl. Electrochem. 29 (1999) 611–617, https://doi.org/10.1023/A:1026423218899.
[14] R. Atkinson, D.L. Baulch, R.A. Cox, J.N. Crowley, R.F. Hampson, R.G. Hynes, M.E. Jenkin, M.J. Rossi, J. Troe, Atmospheric chemistry and physics discussions, Atmos. Chem. Phys. Discuss. 3 (2003) 6179–6699 www.atmos-chem-phys.org/acpd/3/6179/.
[15] J. Martínez, A. Ortiz, I. Ortiz, State-of-the-art and perspectives of the catalytic and electrocatalytic reduction of aqueous nitrates, Appl. Catal. B Environ. 207 (2017) 42–59, https://doi.org/10.1016/j.apcatb.2017.02.016.
[16] N. Barrabés, J. Just, A. Dafinov, F. Medina, J.L.G. Fierro, J.E. Sueiras, P. Salagre, Y. Cesteros, Catalytic reduction of nitrate on Pt-Cu and Pd-Cu on active carbon using continuous reactor: the effect of copper nanoparticles, Appl. Catal. B Environ. 62 (2006) 77–85, https://doi.org/10.1016/j.apcatb.2005.06.015.
[17] A.C.A. De Vooys, R.A. Van Santen, J.A.R. Van Veen, Electrocatalytic reduction of NO_3^- on palladium/copper electrodes, J. Mol. Catal. A Chem. 154 (2000) 203–215.
[18] D. Reyter, D. Bélanger, L. Roué, Elaboration of Cu-Pd films by co-electrodeposition: application to nitrate electro-reduction, J. Phys. Chem. C 113 (2009) 290–297, https://doi.org/10.1021/jp805484t.
[19] B.K. Simpson, D.C. Johnson, Electrocatalysis of nitrate reduction at copper-nickel alloy electrodes in acidic media, Electroanalysis 16 (2004) 532–538, https://doi.org/10.1002/elan.200302790.
[20] J. Sá, D. Gasparovicova, K. Hayek, E. Halwax, J.A. Anderson, H. Vinek, Water denitration over a Pd-Sn/Al_2O_3 catalyst, Catal. Lett. 105 (2005) 209–217, https://doi.org/10.1007/s10562-005-8692-7.
[21] O. Ghodbane, L. Roué, D. Bélanger, Study of the electroless deposition of Pd on Cu-modified graphite electrodes by metal exchange reaction, Chem. Mater. 20 (2008) 3495–3504, https://doi.org/10.1021/cm071815a.
[22] D. Reyter, D. Bélanger, L. Roué, Study of the electro-reduction of nitrate on copper in alkaline solution, Electrochim. Acta 53 (2008) 5977–5984, https://doi.org/10.1016/j.electacta.2008.03.048.
[23] C.J. Mancuso, H.N. Alyea, W.A. Slabaugh, Nitrogen chemistry. E. Nitrites and nitrates, J. Chem. Educ. 45 (1968) A607, https://doi.org/10.1021/ed045pA607.2.
[24] M.-W. Hsieh, T.-J. Whang, Electrodeposition of PdCu alloy and its application in methanol electro-oxidation, Appl. Surf. Sci. 270 (2013) 252–259, https://doi.org/10.1016/j.apsusc.2013.01.012.
[25] L. Mattarozzi, S. Cattarin, N. Comisso, R. Gerbasi, P. Guerriero, M. Musiani, E. Verlato, Electrodeposition of compact and porous Cu-Pd alloy layers and their application to nitrate reduction in alkali, Electrochim. Acta 230 (2017) 365–372, https://doi.org/10.1016/j.electacta.2017.02.012.
[26] C. Xu, Y. Liu, J. Wang, H. Geng, H. Qiu, Nanoporous PdCu alloy for formic acid electro-oxidation, J. Power Sources 199 (2012) 124–131, https://doi.org/10.1016/j.jpowsour.2011.10.075.
[27] Z. Bastl, X-ray photoelectron spectroscopic studies of palladium dispersed on carbon surfaces modified by ions beams and plasmatic oxidation, Collect. Czech. Chem. Commun. 60 (1995) 383–392.
[28] J.C. Bertolini, P. Delichere, B.C. Khanra, J. Massardier, C. Noupa, B. Tardy, Electronic properties of supported Pd aggregates in relation with their reactivity for 1,3-butadiene hydrogenation, Catal. Lett. 6 (1990) 215–224, https://doi.org/10.1007/BF00774723.
[29] L.S. Kibis, A.I. Titkov, A.I. Stadnichenko, S.V. Koscheev, A.I. Boronin, X-ray photoelectron spectroscopy study of Pd oxidation by RF discharge in oxygen, Appl. Surf. Sci. 255 (2009) 9248–9254, https://doi.org/10.1016/j.apsusc.2009.07.011.
[30] Y. Xiong, J. Chen, B. Wiley, Y. Xia, Y. Yin, Z.-Y. Li, Size-dependence of surface plasmon resonance and oxidation for Pd nanocubes synthesized via a seed etching process, Nano Lett. 5 (2005) 1237–1242, https://doi.org/10.1021/nl0508826.
[31] I. Bespalov, M. Datler, S. Buhr, W. Drachsel, G. Rupprechter, Y. Suchorski, Initial stages of oxide formation on the Zr surface at low oxygen pressure: an in situ FIM and XPS study, Ultramicroscopy 159 (2015) 147–151, https://doi.org/10.1016/j.ultramic.2015.02.016.
[32] P. Liu, Z. Cheng, L. Ma, M. Zhang, Y. Qiu, M. Chen, F. Cheng, Cuprous oxide template synthesis of hollow-cubic Cu2O@PdXRuynanoparticles for ethanol electrooxidation in alkaline media, RSC Adv. 6 (2016) 76684–76690, https://doi.org/10.1039/C6RA14439J.
[33] J.F. Moulder, W.F. Stickle, P.E. ' Sobol, K.D. Bomben, J. Chastain, Handbook of X-ray Photoelectron Spectroscopy: A Reference Book of Standard Spectra for Identification and Interpretation of XPS Data, Physical Electronics Division, second ed., Perkin-Elmer Corp., Minesota, 1992.
[34] E.A. Monyoncho, S. Ntais, N. Brazeau, J.J. Wu, C.L. Sun, E.A. Baranova, Role of the metal-oxide support in the catalytic activity of Pd nanoparticles for ethanol electrooxidation in alkaline media, ChemElectroChem 3 (2016) 218–227, https://doi.org/10.1002/celc.201500432.
[35] G. Strukul, R. Gavagnin, F. Pinna, E. Modaferri, S. Perathoner, G. Centi, M. Marella, M. Tomaselli, Use of palladium based catalysts in the hydrogenation of nitrates in drinking water: from powders to membranes, Catal. Today 55 (2000) 139–149, https://doi.org/10.1016/S0920-5861(99)00233-3.
[36] S. Garcia-Segura, M. Lanzarini-Lopes, K. Hristovski, P. Westerhoff, Electrocatalytic reduction of nitrate: fundamentals to full-scale water treatment applications, Appl. Catal. B Environ. 236 (2018) 546–568, https://doi.org/10.1016/j.apcatb.2018.05.041.
[37] U. Prüsse, M. Hähnlein, J. Daum, K.D. Vorlop, Improving the catalytic nitrate reduction, Catal. Today 55 (2000) 79–90, https://doi.org/10.1016/S0920-5861(99)00228-X.
[38] L.A. Estudillo-Wong, E.M. Arce-Estrada, N. Alonso-Vante, A. Manzo-Robledo, Electro-reduction of nitrate species on Pt-based nanoparticles: surface area effects, Catal. Today 166 (2011) 201–204, https://doi.org/10.1016/j.cattod.2010.09.010.
[39] L.A. Estudillo-Wong, G. Santillán-Díaz, E.M. Arce-Estrada, N. Alonso-Vante, A. Manzo-Robledo, Electroreduction of NOx species in alkaline medium on Pt nanoparticles, Electrochim. Acta 88 (2013) 358–364, https://doi.org/10.1016/j.electacta.2012.10.055.
[40] M.P. Pradhan, J.B. Joshi, Absorption of NO_x gases in aqueous NaOH solutions: selectivity and optimization, AIChE J. 45 (1999) 38–50, https://doi.org/10.1002/aic.690450105.
[41] D. Thomas, J. Vanderschuren, Nitrogen oxides scrubbing with alkaline solutions, Chem. Eng. Technol. 23 (2000) 449–455, https://doi.org/10.1002/(SICI)1521-4125(200005)23:5<449::AID-CEAT449>3.0.CO;2-L.
[42] A. Manzo-Robledo, C. Lévy-Clément, N. Alonso-Vante, Electrochemical behavior of nitrogen gas species adsorbed onto boron-doped diamond (BDD) electrodes, Langmuir 23 (2007) 11413–11416, https://doi.org/10.1021/la701875h.
[43] X. Zhang, Nitric oxide (NO) electrochemical sensors, Electrochem. Sens. Biosens. Biomed. Appl. (2008) 1–29, https://doi.org/10.1016/B978-012373738-0.50003-9.
[44] A.C.A. De Vooys, G.L. Beltramo, B. Van Riet, J.A.R. Van Veen, M.T.M. Koper, Mechanisms of electrochemical reduction and oxidation of nitric oxide, Electrochim. Acta 49 (2004) 1307–1314, https://doi.org/10.1016/j.electacta.2003.07.020.
[45] D. Çirmi, R. Aydin, F. Köleli, The electrochemical reduction of nitrate ion on polypyrrole coated copper electrode, J. Electroanal. Chem. 736 (2015) 101–106,

https://doi.org/10.1016/j.jelechem.2014.10.024.
[46] R. Abdallah, F. Geneste, T. Labasque, H. Djelal, F. Fourcade, A. Amrane, S. Taha, D. Floner, Selective and quantitative nitrate electro-reduction to ammonium using a porous copper electrode in an electrochemical flow cell, J. Electroanal. Chem. 727 (2014) 148–153, https://doi.org/10.1016/j.jelechem.2014.06.016.
[47] C. Amatore, J.M. Saveant, Do ECE mechanisms occur in conditions where they could be characterized by electrochemical kinetic techniques? J. Electroanal. Chem. 86 (1978) 227–232, https://doi.org/10.1016/S0022-0728(78)80371-4.